Journal of
Materials Chemistry A

Materials for energy and sustainability

rsc.li/materials-a

ROYAL SOCIETY
OF CHEMISTRY
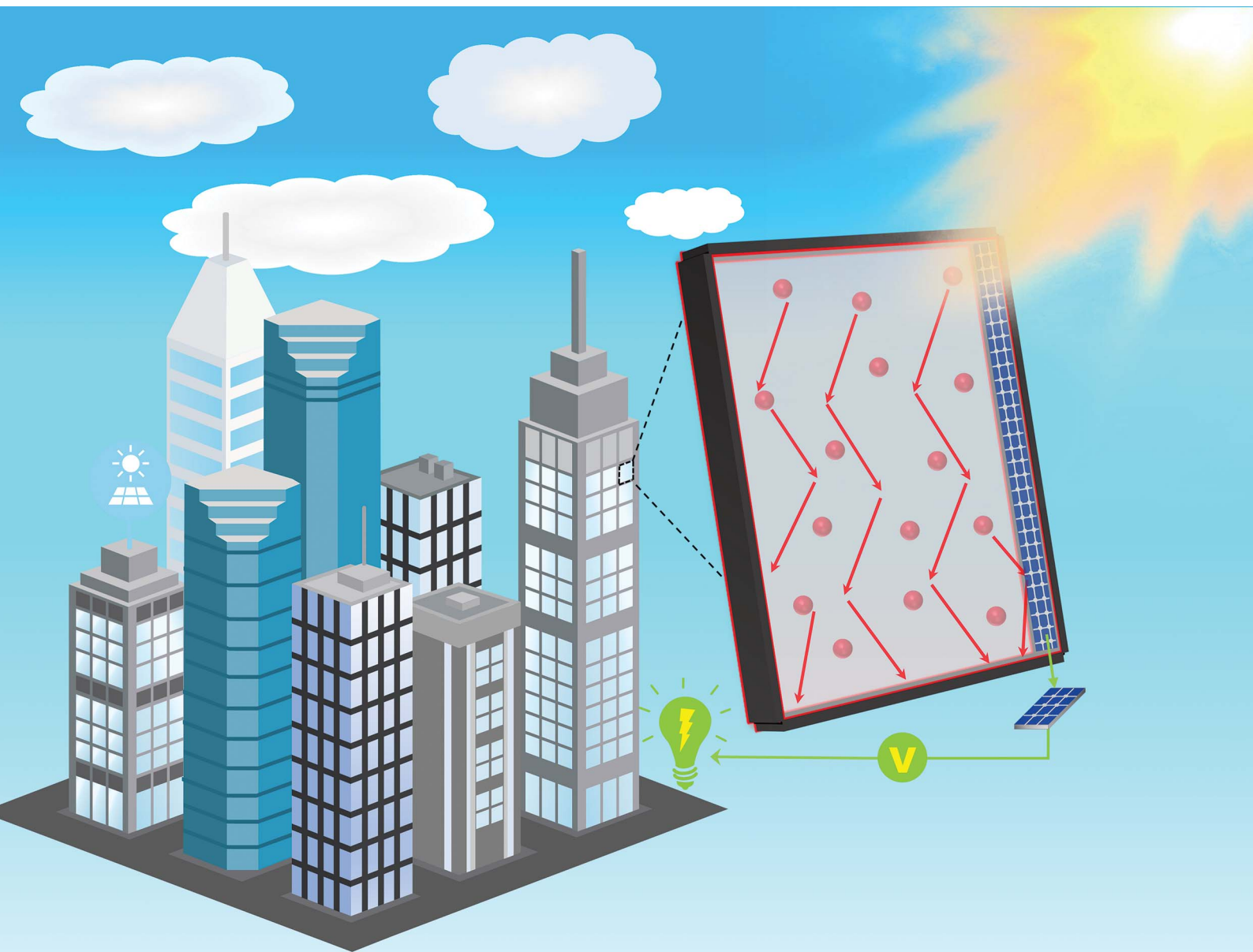
PAPER
Xiao Luo *et al.*
Exploring the optical management and efficiency limit
of luminescent solar concentrators based on advanced
luminophores

Check for updates

Exploring the optical management and efficiency limit of luminescent solar concentrators based on advanced luminophores†

Qi Nie, Wenqing Li, Kuilin Li and Xiao Luo [ID] *

In the context of global warming, luminescent solar concentrators (LSCs) hold great promise as solar windows. Over nearly five decades of development, various suitable luminophores for LSCs, including dye molecules, perovskites and quantum dots, have seen significant advancements. However, the commercialization of LSCs is still immature, and achieving a balance between large area (~ 1 m^2) and high efficiency in laboratory-reported LSCs remains challenging. Consequently, it is important to find more promising luminophores with small reabsorption and high photoluminescence quantum yield (PLQY). In this work, we used Monte Carlo (MC) simulation and recognized calculation formulae to predict the LSCs efficiency of several advanced luminophores of our choice. According to our results, photon-multiplying (PM) LSCs, which include quantum-cutting (QC)-based luminophores and singlet-fission (SF)-based luminophores, hold a promising solution to overcome thermalization loss for high-energy photon excitation for coupled Si-PVs and reduce reabsorption loss. Under the condition of optimal PLQY, the external quantum efficiency of SF-LSCs is expected to exceed 18% even if the area of the LSCs reaches ~ 1 m^2. Considering the thermodynamic concentration limit, PM-LSCs may be better suited for operation under weaker light conditions. We also proposed that tandem LSCs remain an effective approach to maximize efficiency. By employing SF-LSCs as the top layer and CuInSe$_2$/ZnS-based LSCs as the bottom layer, the power conversion efficiency (PCE) of tandem LSCs can reach 11% for an LSC length of 10 cm and 9% for an LSC length of 100 cm under optimal PLQY. Based on the existing material systems, we predict the efficiency bottlenecks in LSCs and provide reliable theoretical support for their commercialization.

Xiao Luo

Prof. Xiao Luo received his B.S. degree in Physics from Sichuan University in 2012 and his PhD in Microelectronics and Solid-State Electronics from Lanzhou University of China in 2017. From 2017 to 2020, he was an assistant professor in the Opto-electronic Materials Dynamics Group at the Dalian Institute of Chemical Physics of China (DICP). He is currently a professor of optoelectronics at the University of Electronic Science and Technology of China (UESTC). His current research focuses on excited state dynamics and optoelectronic applications in low-dimensional materials and hybrid systems.

Introduction

Global warming and the energy crisis are pressing issues around the world, and finding clean and renewable energy is critical. According to a reported work, 40% of global energy consumption and 28% of carbon emissions are contributed by buildings.[1,2] The design concept of luminescent solar concentrators (LSCs) aligns well with building integrated photovoltaics (BIPVs). LSCs are considered one of the best choices of devices for solar windows, which are transparent (or semitransparent) and inexpensive. The schematic principle of the LSC-PV system is shown in Fig. 1a, and the system simply consists of lumino-phores, a waveguide medium, and four PV cells. The light concentrating process of LSCs can be divided into the following steps: when the incident photons reach an LSC, some photons are absorbed by luminophores and new photons are emitted, according to their emission spectra (step 1 in Fig. 1a), and the remaining photons that are not absorbed are transmitted out

School of Optoelectronic Science and Engineering, University of Electronic Science and Technology of China (UESTC), Chengdu 610054, PR China. E-mail: luox@uestc.edu.cn
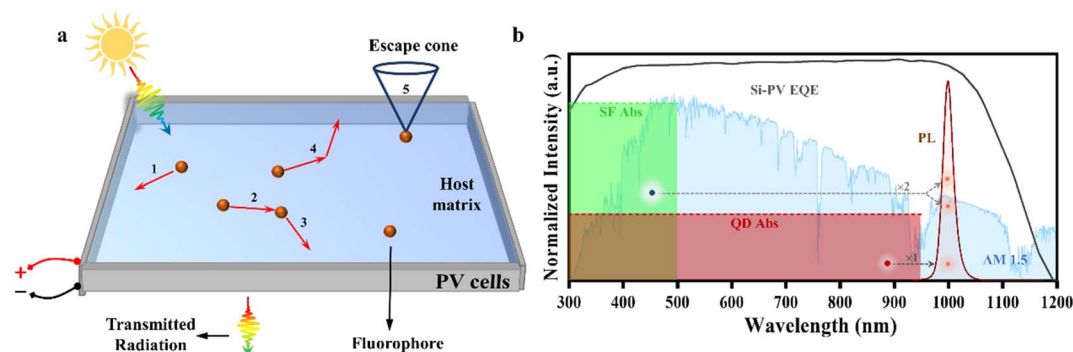
Fig. 1 (a) Schematic depiction of the LSC–PV systems studied in this work. The device is supplemented by edge-mounted PVs. (b) Optimal spectral for tandem LSC luminophores. The green area represents the absorption of SF materials, and the materials can emit two low-energy photons after absorbing one high-energy photon. The red area represents the absorption of QD materials that can absorb the photons before 950 nm. The PL spectral represents a suitable PL region for Si-PV cells. The AM 1.5 solar spectrum is superimposed in blue. The black curve is the EQE of the Si-PV cells.

from the bottom surface. For the emitted photons in the waveguide medium, some of them enter the escape cone and then escape (step 5 in Fig. 1a), some of them are reabsorbed by the luminophores (step 2 in Fig. 1a), and the others may reach the LSC's edges directly. For the reabsorbed photons, the luminophores may re-emit new photons depending on their photoluminescent quantum yields (PLQYs) (step 3 in Fig. 1a). After going through the above processes, some of these photons reach the LSC's edges and are absorbed by coupled solar cells to produce energy.

Since the LSC was proposed by Weber and Lambe in 1976 first,[3] the luminophore system of LSCs grew dramatically within fifty years of development. The luminophores of LSCs contain dye molecules, colloidal quantum dots (QDs), various nanocrystals (NCs) and so on. Highly efficient PLQY and large Stokes shifts of light-emitting cluster materials are always the goals pursued by LSCs. From the initial use of rhodamine 6G or its derivatives as the luminophores[4] to chalcogenide core/shell QDs,[5] the advancement of LSCs has seen a gradual pace over the first three decades of development. However, for the last decade, LSCs have witnessed a vigorous burst and a vast amount of new materials have been reported. Many novel organic molecule-based LSCs, including thermally activated delayed fluorescence dye,[6] aggregation-induced emission molecule[7,8] and fluorescence resonance energy transfer complex,[9–11] have achieved relatively excellent performance. Among molecule-based LSCs, a promising power conversion efficiency (PCE) of 2.6% was reported by Zhang et al., and the length of their large-area LSC was 20 cm.[10] For perovskite NCs, despite their excellent luminescent properties, reabsorption remained a hindrance until quantum-cutting (QC) was first introduced for LSC applications by Luo et al.[12] The $CsPbCl_3$:-Yb^{3+}-based LSCs (25 cm^2) had an internal quantum efficiency of up to 118%, but the weaker absorption efficiency affected their performance. Subsequently, Cohen et al. proposed that using $CsPbCl_xBr_{3-x}$:Yb^{3+}-based LSCs can further improve the absorption efficiency of QC-based LSCs.[13] Due to the theoretically optimal PLQY of 200%, the QC luminophores can be

considered one of the photon-multiplying (PM) materials. Recently, non-toxic luminophore materials, such as I–III–VI ternary QDs[14] and carbon dots (CDs), have become the research hotspot. Wu et al. used $CuInSe_2$/ZnS QDs as the luminophore of bottom layer LSCs of their tandem system and achieved 3.1% of PCE when their length of LSCs was 15.24 cm.[15] Gungor et al. reported that their Zn-doped core/shell $CuInSe_{2-x}S_x$/$CuInS_2$-based LSCs had an external quantum efficiency of 11.8% when the length of the LSC was 9.5 cm.[16] It is the highest external quantum efficiency under the standard AM 1.5 solar spectrum reported so far. More recently, Park et al. introduced a new structure in $CuInS_2$/ZnS based LSC where a patterned low-refractive-index medium acted as an optical 'guard rail' to reduce reabsorption loss.[17] They achieved external quantum efficiencies of 45% for a 100 cm^2 area under 405 nm excitation. CD-based LSCs have many advantages, such as being stable, nontoxic, earth-abundant and low-cost.[18,19] However, we found that many of the reported CD-based LSCs with high efficiency are very small in size due to their relatively large reabsorption.[20–25] To address this issue, Gong et al. proposed using barium-doped CDs with a Stokes shift of 0.68 eV and PLQY of 80.81% to build large-area LSC until very recently and achieved a breakthrough optical conversion efficiency of 7.16% and PCE of 6.87% under natural light irradiation (40 mW cm^{-2}).[26] We also observed some luminophore systems with great potential for LSCs, such as molecular triplet energy transfer (TET) to QDs or ions for luminescence. This system of singlet fission (SF) can be considered another PM material. Rao et al. proposed that using SF could improve efficiency by overcoming thermalization loss in applications of photovoltaics.[27] Gray et al. achieved the TET from 6,11-bis[(triisopropylsilyl) ethynyl]tetracene-2-methylthiol to PbS QDs.[28] The triplet yield from singlet fission was calculated as 130% ± 10%, and the internal triplet transfer efficiency was close to unity. In their subsequent work, they proposed the ligand-directed self-assembly of organic-QD blend films with an SF efficiency of 186% ± 18%, while the whole PLQY system was 24.5%.[29] Very recently, Baikie et al. proposed PM technologies for LSCs,[30] and

19900 | J. Mater. Chem. A, 2024, 12, 19899–19909

This journal is © The Royal Society of Chemistry 2024

they suggested that using PbS with tetracene ligands attached could provide considerable efficiency in the application of LSCs. However, for systems with tetracene-anchored PbS NCs, there is absorption competition between QDs and tetracene, making it challenging to control the concentration ratio between the components. This results in the relatively low PLQY of the whole system because the luminescence of the QDs comes partly from the intrinsic transition of QDs and partly from the molecular TET following the SF process. Interestingly, Han *et al.* achieved the energy transfer from the triplet of tetracene to Yb^{3+} of $NaGdF_4$:Yb NCs for luminescence,[31] but the PLQY was not reported. Because $NaGdF_4$:Yb NCs have only a very small absorption in the range of the solar spectrum, the luminescence of Yb^{3+} is mainly dominated by the molecular SF process.

In the context of BIPVs, the LSC-PV system should be regarded as a whole device. Consequently, the efficiency and absorption regions of coupled solar cells are of vital importance. Given that silicon-based photovoltaic (Si-PV) cells have reached a mature and commercialized stage, and their high external quantum efficiency (EQE) region covers the wavelength ranging from 300 to 1100 nm (as indicated by the grey curve in Fig. 1b), we choose to focus on Si-PVs as the stationary component in our discussion.[32] Considering the bandgap of silicon ($\sim$1.1 eV), to maximize the conversion of solar energy, the PL emission of LSC luminophores should be close to $\sim$1000 nm. This ensures sufficient photon absorption and matches the high EQE range of Si-PV cells. However, for narrow bandgap luminophores, the process of absorbing high-energy photons and then emitting near-infrared light results in thermalization losses in the LSC-PV system. Given that SF materials exhibit effective sunlight absorption of up to $\sim$500 nm and can overcome thermalization losses by multiplying luminescence, we propose an optical management scheme for tandem LSCs (Fig. 1b), which effectively mitigates the contradiction between absorption efficiency and thermalization losses. These tandem LSCs are constructed by SF luminophore-based LSCs as the top layer (green region in Fig. 1b) and narrow bandgap luminophore-based LSCs as the bottom layer (red region in Fig. 1b).

In this work, we identify six representative materials that hold significant promise in the current stage of LSC research. These materials include $CsPbCl_3$:Yb^{3+} NCs, $CsPbCl_xBr_{3-x}$:Yb^{3+} NCs and $NaGdF_4$:Yb–tetracene NCs, serving as the PM materials. Additionally, we analyze Mn^{2+}-doped Cd_xZn_{1-x}S/ZnS QDs with negligible reabsorption, $CuInSe_2$/ZnS QDs with broad absorption and a larger Stokes shift, and non-toxic CDs. We use Monte Carlo (MC) simulation and recognized methods of calculation to predict the different LSC parameters, such as external quantum efficiency (η_{ext}), internal quantum efficiency (η_{int}) and concentration factor (C). For luminophores with unavoidable reabsorption, such as $CuInSe_2$/ZnS QDs and red CDs, the constructed LSCs by them exhibit competitiveness in small-size LSCs. For luminophores with negligible reabsorption, they are quite suitable for large-area LSCs. Under optimal PLQY, $NaGdF_4$:Yb–tetracene-based LSCs can achieve a size-independent superior η_{ext} of 18.8%, which is much higher than the efficiency reported so far. We adopt $NaGdF_4$:Yb–tetracene-based LSCs and $CuInSe_2$/ZnS QD-based LSCs to

construct a system of tandem LSCs. The η_{ext} of the tandem system reaches 27.6% for $L = 10$ cm, and the PCE exceeds 11% under optimal PLQY. In addition, the PCE reaches $\sim$9% when $L = 100$ cm due to the reabsorption of the bottom layer of tandem LSCs. In the context of commercialized silicon-based cells, our simulation results demonstrate the efficiency bottleneck of LSCs at this stage and provide reliable theoretical support for their commercialization.

Experimental

(I) Synthesis of $NaGdF_4$:Yb NCs

$NaGdF_4$:Yb NCs were synthesized by hot-injection following procedures reported by Han *et al.*[31] A water solution (2 mL) containing $Gd(Ac)_3$ (0.2 mmol) and $Yb(Ac)_3$ (0.2 mmol) was mixed with oleic acid (3.5 mL) and 1-octadecene (10.5 mL) in a 50 mL flask, followed by heating at 150 °C for 2 h. Thereafter, the reactant was cooled to 50 °C, and a methanol solution (6 mL) containing NH_4F (1.36 mmol) and NaOH (1 mmol) was added. The mixed solution was stirred for 30 min. The reaction temperature was then increased to 100 °C to remove the methanol from the reaction solution. After that, the reactant was heated at 270 °C under a nitrogen atmosphere for 1 h, followed by cooling to room temperature. The target product is obtained by centrifuging.

(II) Synthesis of $CsPbCl_3$:Yb^{3+} NCs

$CsPbCl_3$:Yb^{3+} NCs were synthesized by hot-injection following the procedures reported by Luo *et al.*[12] Briefly, 5.0 mL 1-octa-decene, 0.5 mL oleyl amine, 1.0 mL oleic acid, 0.2 mmol $Pb(OAc)_2\cdot 3H_2O$, 280 μL of 1 M CsOAc in ethanol, and 0.16 mmol $Yb(OAc)_3\cdot xH_2O$ were loaded into a 50 mL flask. The solution was degassed at room temperature for 5 min and at 110 °C for 1 hour. The reaction was then switched to an N_2 atmosphere and heated to 240 °C. At this temperature, 0.2 mL chloro-trimethylsilane (TMS-Cl) in 0.5 mL 1-octadecene was swiftly injected. The target product is obtained by cooling the flask rapidly and centrifuging.

(III) Synthesis of $CsPbCl_xBr_{3-x}$:Yb^{3+} NCs

$CsPbCl_xBr_{3-x}$:Yb^{3+} NCs were obtained by anion exchange reported by Milstein *et al.*[33] Briefly, the as-synthesized $CsPbCl_3$:Yb^{3+} NCs were dissolved in hexane, and the bromotrimethylsilane (TMS-Br) was added to the reaction under nitrogen atmosphere until the onset of absorption of the sample reached 490 nm.

(IV) Synthesis of $CuInSe_2$/ZnS QDs

$CuInSe_2$/ZnS QDs were synthesized by hot injection following procedures reported by Wu *et al.*[15] 0.6 mmol $In(Ac)_3$, 0.6 mmol CuI, 6 mL oleyl amine and 6 mL 1-octadecene were loaded into a three-neck flask, heated to 100 °C and degassed for 30 min. The mixture was then heated to 210 °C under N_2 atmosphere. Next, by dissolving 1.2 mmol Se pellets in 3 mL oleyl amine and 0.9 mL diphenylphosphine, the Se-solution was injected into the above mixture at 210 °C. The reaction was heated to 230 °C

This journal is © The Royal Society of Chemistry 2024

J. Mater. Chem. A, 2024, **12**, 19899–19909 | **19901**

for ZnS shell growth. The ZnS-solution was prepared by dissolving 5 mmol Zn(St)$_2$ in 10 mL 1-octadecene, 5 mL oleic acid and 5 mL dodecanethiol at 150 °C for 10 min. The solution was injected in the CuInSe$_2$ core solution at 2 h intervals between each injection and 2 mL per injection. After the last injection, the reaction was kept at 230 °C for 4 h. The target product was obtained by cooling the flask rapidly and centrifuging.

(V) Synthesis of Cd$_x$Zn$_{1-x}$S/ZnS QDs

5 mL dodecanethiol and 10 mL 1-octadecene were loaded into a three-neck flask and kept under vacuum at 40 °C for 1 h, which was then cooled to room temperature and changed to N$_2$ atmosphere. 5 mL of the Zn-solution (1 mmol Zn(OAc)$_2$·2H$_2$O dissolved in 0.8 mL oleyl amine and 9.2 mL 1-octadecene), 5 mL of the Cd-solution (1 mmol CdO dissolved in 2 mL oleic acid and 8 mL 1-octadecene), 5 mL of the Mn-solution (0.05 mmol Mn(OAc)$_2$·4H$_2$O dissolved in 1 mL oleyl amine and 9 mL 1-octadecene) and 5 mL of the S-solution (4.0 mmol S powder dissolved in 10 mL 1-octadecene) were added to the flask and heated to 230 °C under N$_2$ atmosphere. The mixture was kept at this temperature for 1 min. Then, 15 mL of the Zn-solution (4 mmol Zn(OAc)$_2$·2H$_2$O dissolved in 3 mL oleyl amine and 7 mL 1-octadecene) was added dropwise into the reaction mixture six times (2.5 mL per time) at 10 min intervals. The target product is obtained by cooling the flask rapidly after 10 min reaction and centrifuging.

(VI) Synthesis of red CDs

Red CDs were prepared by solvothermal synthesis using the literature method.[34] 10 mg 1,3-dihydroxynaphthalene and 40 mg KIO$_4$ were dissolved in ethanol (10 mL), and the solution was then transferred to a poly(tetrafluoroethylene) (Teflon)-lined autoclave (25 mL) and heated at 180 °C for 1 h. The target product is obtained by cooling naturally and purifying via silica column chromatography using a mixture of methyl alcohol and dichloromethane as the eluent.

Results and discussion

(I) The luminophores of LSCs

To explore the possible future optimal efficiency of LSCs in this field of solar windows, in this work, we select the following six highly promising materials for our analysis: CsPbCl$_3$:Yb^{3+} NCs, CsPbCl$_x$Br$_{3-x}$:Yb^{3+} NCs, CuInSe$_2$/ZnS QDs, Mn^{2+}-doped Cd$_x$-Zn$_{1-x}$S/ZnS QDs, red CDs and NaGdF$_4$:Yb–tetracene NCs. The absorption and emission spectra of NaGdF$_4$:Yb–tetracene NCs and CuInSe$_2$/ZnS QDs are shown in Fig. 2a. The absorption and emission spectrum of CsPbCl$_3$:Yb^{3+} NCs, CsPbCl$_x$Br$_{3-x}$:Yb^{3+} NCs, Mn^{2+}-doped Cd$_x$Zn$_{1-x}$S/ZnS QDs and red CDs are shown in Fig. S1a–d,† respectively.

For the Yb^{3+}-doped luminophores, we categorize both QC-based LSCs and SF-based LSCs as PM-LSCs. The PM-LSCs imply that, under ideal conditions, these materials can absorb one high-energy photon and subsequently emit two low-energy photons, thereby increasing the theoretical limit of PLQY to 200%. These materials reduce thermalization losses, make the

Stokes shift of the luminophores increase greatly in the process of energy transfer, and achieve negligible reabsorption. These advantages make PM materials one of the most promising candidates for LSCs. The emissive $2F_{5/2} \rightarrow 2F_{7/2}$ f–f transition of Yb^{3+}, which has an energy gap (E_{f-f}) of ~1.25 eV, matches the high-efficiency region of commercialized silicon-based PV cells. The energy gaps (E_g) of CsPbCl$_3$ NCs and CsPbBr$_3$ NCs are ~3.05 eV and ~2.39 eV, respectively. According to the law of conservation of energy, the energy bandgap consistent with $E_g >$ E_{f-f} of the CsPbCl$_x$Br$_{3-x}$ NCs can be used as carriers for QC.[33] Therefore, based on our previous work in which we first introduced the QC materials into LSCs,[12] we choose the CsPbCl$_3$:Yb^{3+} NCs and CsPbCl$_x$Br$_{3-x}$:Yb^{3+} NCs with the E_g of ~2.53 eV for use in simulations to predict the optimal efficiency of LSCs.

For SF-based LSCs, we tend to choose NaGdF$_4$:Yb–tetracene NCs as the luminophores for analysis. In the study by Han et al., they demonstrated that triplet energy can be transferred to Yb^{3+} luminescence based on NaGdF$_4$:Yb–tetracene NCs.[31] In the progress of SF, a photogenerated singlet exciton (S$_1$) is converted into two triplet excitons (T$_1$). Intriguingly, SF also proceeds very efficiently in endothermic systems, where $E(S_1) <$ $2 \times E(T_1)$, which overcomes energy barriers ($E_b = 2E(T_1) - E(S_1)$) of up to 200 meV.[35] Therefore, the cutoff of the absorption spectrum of tetracene is close to 540 nm (as shown in Fig. 2a), which provides an appreciable absorption efficiency for its use as the LSC luminophores. In contrast, CsPbCl$_x$Br$_{3-x}$:Yb^{3+} NCs can absorb only the solar photons before ~490 nm. These results show that NaGdF$_4$:Yb–tetracene NCs are very promising materials for LSC applications and are better than QC-based LSCs.

Excluding PM-LSCs, research in this field has predominantly focused on luminophores with minimal reabsorption. Mn^{2+}-doped QDs are the solution used to increase the Stokes shift and achieve no reabsorption. Consequently, we chose Mn^{2+}-doped Cd$_x$Zn$_{1-x}$S/ZnS QDs as an analytical sample, as reported by Wu et al.[15] However, the efficiency of solar energy absorption leads to their limitation as the LSC luminophores. Instead, copper-based ternary QDs provide sufficient absorption efficiency. Although their reabsorption is rather small, the loss of reabsorption is unavoidable as the size of the LSCs increases. We selected CuInSe$_2$/ZnS QDs, which have a large absorption efficiency of solar energy, for our evaluation. Recently, in light of the growing interest in environmentally friendly and sustainable materials within the scientific community, CDs have emerged as promising new materials without toxicity. Numerous studies have demonstrated that CDs can serve as efficient luminophores for LSCs. Consequently, we included red CDs as one of our predicted luminophores for use. The red CDs have an absorption onset of 700 nm and an emission center wavelength of 599 nm. Large reabsorption is an unavoidable problem for this class of materials.

(II) Optimal concentration of luminophores

The key parameters commonly associated with LSCs include η_{int}, η_{ext}, C, and external quantum efficiency for PV-LSC systems (EQE$_{LSC-PV}$) and PCE. Klimov et al. derived expressions for each

19902 | J. Mater. Chem. A, 2024, 12, 19899–19909
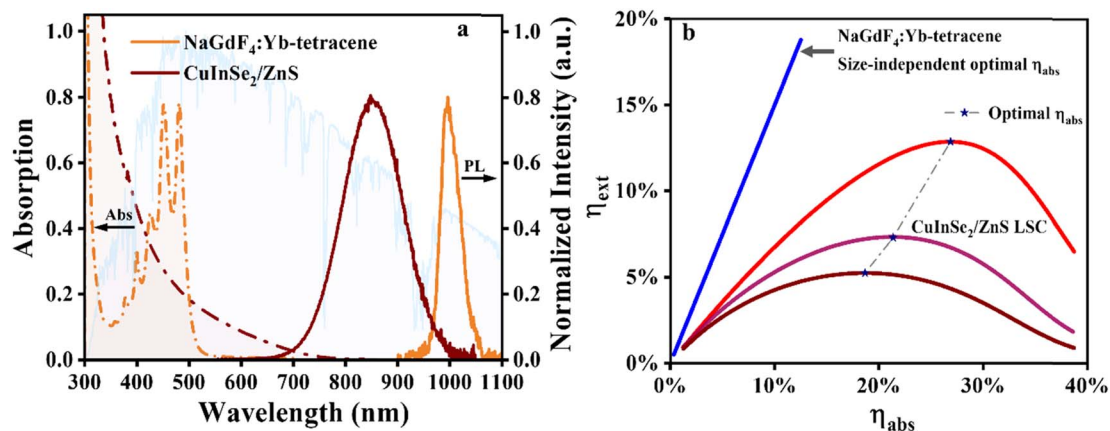
This journal is © The Royal Society of Chemistry 2024

Fig. 2 (a) Absorption and PL spectra for CuInSe$_2$/ZnS QDs (red-brown lines) and NaGdF$_4$:Yb−tetracene NCs (orange lines). (b) Extrapolated η_{abs}-dependent η_{ext} for CuInSe$_2$/ZnS QD-based LSCs (red, purple and brown lines) and NaGdF$_4$:Yb−tetracene NC-based LSCs (blue line). The NaGdF$_4$:Yb−tetracene NC-based LSCs have size-independent optimal η_{abs}. The red line represents a size of 10 cm, the purple line represents a size of 50 cm, and the brown line represents a size of 100 cm for CuInSe$_2$/ZnS QD-based LSCs.

parameter of LSCs under ideal conditions of single-wavelength excitation.[36] In this work, we discuss the theoretical efficiency that can be achieved by the LSCs under the conditions of practical application and the irradiation of the AM 1.5 solar spectrum ($S_{in}(\lambda)$). Therefore, we take the wide spectrum of conditions and the scattering coefficient (s) into consideration. The spectral averaging equations are expressed as follows:

$$\eta_{abs} = \frac{\int [1 - R][1 - e^{-\alpha(\lambda)d}] S_{in}(\lambda) d\lambda}{\int S_{in}(\lambda) d\lambda}, \quad (1)$$

$$\eta_{int} = \frac{\int \eta_{PL} \eta_{trap} \left[1 + \beta[\alpha(\lambda) + s] L \left(1 - \frac{\alpha(\lambda)\eta_{PL} + s}{\alpha(\lambda) + s} \eta_{trap} \right) \right]^{-1} \Phi_{PL}(\lambda) d\lambda}{\int \Phi_{PL}(\lambda) d\lambda} \quad (2)$$

$$\eta_{ext} = \frac{\int [1 - R][1 - e^{-\alpha(\lambda)d}] S_{in}(\lambda) d\lambda}{\int S_{in}(\lambda) d\lambda} \frac{\int \eta_{PL} \eta_{trap} \left[1 + \beta[\alpha(\lambda) + s] L \left(1 - \frac{\alpha(\lambda)\eta_{PL} + s}{\alpha(\lambda) + s} \eta_{trap} \right) \right]^{-1} \Phi_{PL}(\lambda) d\lambda}{\int \Phi_{PL}(\lambda) d\lambda}, \quad (3)$$

where R is the surface reflection coefficient, η_{PL} is the PLQY and η_{trap} is the efficiency of photons entering total internal reflection. Then, C can be calculated using $C = G\eta_{ext}$ according to eqn (3). In eqn (1)–(3), $\alpha(\lambda)$ and $\Phi_{PL}(\lambda)$ represent the absorption and fluorescence spectra of luminescent materials, respectively; and $S_{in}(\lambda)$ is the solar photon flux. In Klimov's work,[36] they proved that $\beta = 1.4$ is suitable for the computational prediction of LSCs of small size and $\beta = 1.8$ is suitable for the computational prediction of LSCs of large size. He also used the expression $\beta = 1.4 + 0.5(L/150)^{1/2}$ to obtain a perfect match to their MC simulation results across the range of distance $L = 0$–2000 cm, which

leads to unphysical behavior at very large L. In this work, the L of LSCs ranges from $L = 5$–150 cm. We therefore applied the above expression of the β values to match the model of our MC simulation.

Liu *et al.* categorized LSCs according to their structure into full polymer LSCs, top-coated thin film LSCs, liquid LSCs and laminated LSCs.[37] We can analyze the different structures of LSCs by calculating the effective absorption coefficient and transforming them into the structure of full polymer LSCs. Consequently, in this work, we use a full polymer LSC with a thickness of $d = 0.5$ cm as the model for the analysis. The L of LSCs varies from 5 to 150 cm. We emphasize that the LSCs with a special waveguide structure are not within the scope of discussion in this work.

Then, we calculated the spectral data of the six lumino-phores to determine the optimal concentration of different LSCs. Under optimal PLQY and ideal situation without scattering, we find that NaGdF$_4$:Yb−tetracene-based LSCs have size-independent optimal η_{abs} due to their no reabsorption and η_{ext} has a linear relationship with η_{abs}, which is shown as a blue line in Fig. 2b. The QC-LSCs and Mn^{2+}-doped Cd$_x$Zn$_{1-x}$S/ZnS-based LSCs governed by the same rule and the results are shown in Fig. S2a–c.† Therefore, we choose the maximum η_{abs} of the four luminophores for use in this work. For CuInSe$_2$/ZnS-based LSCs, as the value of L increases, the optimal η_{abs} decreases progressively (as depicted in Fig. 2b). This phenomenon arises because higher η_{abs} values lead to increased reabsorption losses in large-area LSCs, resulting in the existence of an optimal point

This journal is © The Royal Society of Chemistry 2024

J. Mater. Chem. A, 2024, **12**, 19899–19909 | **19903**

for η_{abs}. Red CD-based LSCs have a similar tendency, as shown in Fig. S2d.† Our investigation reveals that the optimal η_{abs} for red CD-based LSCs exhibits a more rapid decline compared to CuInSe$_2$/ZnS-based LSCs. Specifically, this trend indicates that as reabsorption increases, the size-dependent η_{abs} experiences a faster decrease. We also calculate the results under the situation that considers the scattering and unideal PLQY. According to the study of Wu *et al.*, their LSCs have a scattering factor of 0.012 cm^{-1}, which represents some of the possible shortcomings of existing preparation processes.[15] Therefore, we set the scattering factor to be 0.012 cm^{-1}, and the results are shown in Fig. S3 and S4.† The size-dependent η_{ext} decreases as the L increases for the six materials. In particular, for NaGdF$_4$:Yb–tetracene-based LSCs, the optimal η_{ext} decreases from 16.15% to 10.95% when the L increases from 10 cm to 100 cm under the condition that the PLQY is 180% and the scattering factor is 0.012 cm^{-1}. Moreover, QC-based LSCs and Mn^{2+}-doped Cd$_x$-Zn$_{1-x}$S/ZnS-based LSCs have a similar tendency. Hence, optimizing the PLQY of the luminophores and refining the fabrication processes are crucial for the practical application of LSCs.

(III) MC simulation results for LSCs

To estimate the performance of six luminophore-based LSCs, we build an appropriate MC simulation model for all the luminophores. We used the mentioned LSC model, and the details of the MC simulation are described in the ESI.† First, we simulate the ideal PLQY situation using optimal η_{abs}, and we set the number of incident photons to be 10^6, which is enough to get stabilized results. The simulation result plots of 10 cm-LSC, as well as the photon going statistics are displayed in Fig. 3 and S5,† respectively. The brown statistic graphs represent the destination of the incident photons, which can demonstrate the absorption capacity of different luminophores (Fig. 3b and e). The green statistic graphs represent the destination of the photons emitted by the luminophores, which demonstrates the efficiency of photon transfer to the edges (η_{edge}) (Fig. 3c and f). According to the density of outgoing photons at the edges of the ray tracing schematic of LSCs (Fig. 3a, d, S5a, d, g and j†), NaGdF$_4$:Yb–tetracene-based LSCs and CuInSe$_2$/ZnS-based LSCs have excellent η_{ext} than other luminophores-based LSCs. The CuInSe$_2$/ZnS-based LSCs and red CD-based LSCs have relatively low η_{edge}, which are 51.81% and 39.8% due to their reabsorption, respectively. Other luminophore-based LSCs have the η_{edge} approach of 75% due to their negligible reabsorption. Then, we simulate the 100 cm LSCs under an ideal situation, as shown in Fig. S6.† The η_{edge} of CuInSe$_2$/ZnS-based LSCs decreases to 22.59%, and the η_{edge} of red CD-based LSCs decreases to 6.57%. For the other four luminophores without absorption, the efficiency remains unchanged when the L enlarges. Second, the unideal PLQY situation and scattering factor are included in the discussion. The MC simulation results are shown in Fig. S7 and S8,† and the trends in efficiency are consistent with the previous section. All the results demonstrate that the NaGdF$_4$:Yb–tetracene-based LSCs are the most promising luminophores in the large-area LSCs, and CuInSe$_2$/ZnS-based LSCs have excellent efficiency in relatively small-area LSCs.

To better show the performance of each important parameter of LSCs under the situation of considering the scattering factor, we set the PLQY as 200%, 180% and 160% for three PM luminophores and the scattering factor as 0.012 cm^{-1}. For the other three luminophores, we set the PLQY to be 100%, 80% and 60%. The results of η_{int} as well as the η_{ext} of the LSCs of the six luminophores are shown in Fig. S9–S14.† The η_{int} and η_{ext} of the LSCs of all the six luminophores decreases with increasing size, but the rate of decrease varies depending on the
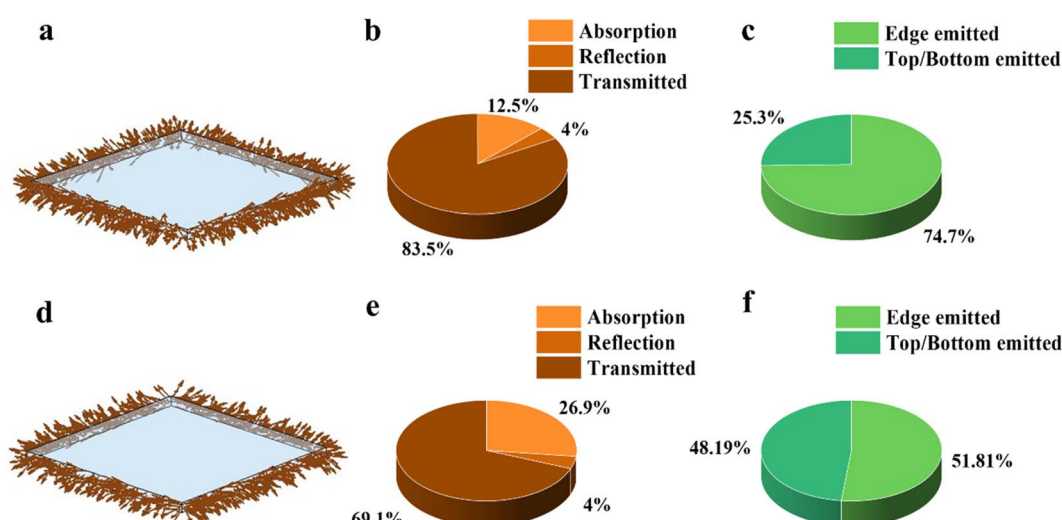

Fig. 3 Monte Carlo ray-tracing simulations for NaGdF$_4$:Yb–tetracene NC-based LSCs and CuInSe$_2$/ZnS QD-based LSCs with a dimension of 10 × 10 × 0.5 cm^3 under ideal situation. (a) Light simulation diagram of NaGdF$_4$:Yb–tetracene NC-based LSCs. (b) Statistical diagram of incident photons of NaGdF$_4$:Yb–tetracene NC-based LSCs. (c) Statistical diagram of emitted photons of NaGdF$_4$:Yb–tetracene NC-based LSCs. (d) Light simulation diagram of CuInSe$_2$/ZnS QD-based LSCs. (e) Statistical diagram of incident photons of CuInSe$_2$/ZnS QD-based LSCs. (f) Statistical diagram of emitted photons of CuInSe$_2$/ZnS QD-based LSCs.

19904 | *J. Mater. Chem. A*, 2024, **12**, 19899–19909

This journal is © The Royal Society of Chemistry 2024

differences in luminophore's reabsorption. To visually describe the variation of η_{int} and η_{ext} with L, we first obtain two predictive curves by changing the β and length in eqn (1) and (2). Based on the results obtained from the six luminophores (as depicted in Fig. S9–S14†), the two dashed lines in each case correspond to the calculated outcomes for β values of 1.4 and 1.8, respectively. Notably, we observed that all the MC simulation results fell within the range defined by these two dashed curves, but they did not precisely align with the calculated results. We then set the value of β as $\beta = 1.4 + 0.5(L/150)^{1/2}$, and we obtained a new solid that can perfectly match our MC simulation results for all the six luminophores (Fig. S9–S14†). The PLQY plays a critical role in determining the η_{int} and η_{ext}. For CuInSe$_2$/ZnS-based LSCs (shown in Fig. S9†), as the value of PLQY increases from 60% to 100%, there is a substantial increase in η_{int} and η_{ext} over the entire range of L. Notably, when the PLQY reaches 100%, both η_{int} and η_{ext} are approximately twice as high as when the PLQY is 60%. For instance, at an L of 5 cm, the η_{int} is 52.92% and η_{ext} is 14.56%. However, as the LSC size increases (*e.g.*, $L = 150$ cm), the η_{int} decreases to 8.86%, and η_{ext} reduces to 2.43%. These findings highlight that even for copper-based ternary quantum dots with relatively low reabsorption, efficiency decline remains significant in large LSCs. For red CD-based LSC (shown in Fig. S10†), the η_{int} and η_{ext} decay at a faster rate than CuInSe$_2$/ZnS-based LSCs with increasing L. We believe that this is because the reabsorption of red CDs is much greater than that of the CuInSe$_2$/ZnS QDs. For luminophores without reabsorption losses, the L-dependence of the η_{int} and η_{ext} are only related to the scattering factor. Even though the scattering factor is only 0.012 cm^{-1}, the efficiency of these luminophore-based LSCs still decays very badly (Fig. S11–S14†). This means that the process is equally crucial for preparing large-area LSCs. All the results under optimal PLQY and a scattering factor of 0.012 cm^{-1} are shown in Fig. S15.†

We summarized the MC simulation results and computational predictions for the six luminophores under the ideal case, as depicted in Fig. 4. For the η_{ext}, we find that NaGdF$_4$:Yb–tetracene-based LSCs have the best η_{ext} of 18.8% in all the sizes of LSCs. It is much higher than the QC-based LSCs due to its excellent ability of absorption. We can emphasize that the NaGdF$_4$:Yb–tetracene is a very promising luminophore for LSCs if we can optimize its PLQY to the limit. For the CuInSe$_2$/ZnS-based LSCs, it is still an excellent material for luminophore at this stage due to its large Stokes shift and very strong light-absorbing capacity. In a relatively small area, the CuInSe$_2$/ZnS-based LSCs can achieve higher η_{ext} than the CsPbCl$_x$Br$_{3-x}$:Yb^{3+}-based LSCs.

For the concentrating factor, we can observe from Fig. 4b that the CuInSe$_2$/ZnS and red CDs with reabsorption loss show saturation with increasing LSC size. For the other four luminophores without reabsorption loss, none of them saturated in the range of LSC sizes we simulated. It is worth noting that C quantifies the real increase in the electrical power output compared to the original PV cell. If $C > 1$, we can assume that the current of the PV cells increases under the action of an LSC. Red CD-based LSCs show a small concentration factor that is smaller than 1 due to their large reabsorption. This means that the red CDs may not be suitable for constructing LSC. Moreover, CuInSe$_2$/ZnS-based LSCs show their potential to achieve a concentration larger than 1 because of their high η_{abs} and relatively small reabsorption. Consequently, luminophores with reabsorption make it difficult to achieve a large concentration factor. The concentration factor of CsPbCl$_3$:Yb^{3+} NC-based LSCs and Mn^{2+}-doped Cd$_x$Zn$_{1-x}$/ZnS-based LSCs can reach ∼3 when the L is 150 cm due to their poor absorption of solar energy. If the scattering factor is considered, both of the two LSCs have a concentration factor of ∼1 when the L is 150 cm (Fig. S15b†). Notably, CsPbCl$_x$Br$_{3-x}$:Yb^{3+} NC-based LSCs and NaGdF$_4$:Yb–tetracene-based LSCs show their powerful potential to achieve large concentration factors in the large LSC devices. For NaGdF$_4$:Yb–tetracene-based LSCs, factor C can exceed 10.

Next, we analyze the thermodynamic limits of the aforementioned LSCs. Based on the second law of thermodynamics, Eli Yablonovitch[38] derived the formula of thermodynamic limit C as follows:
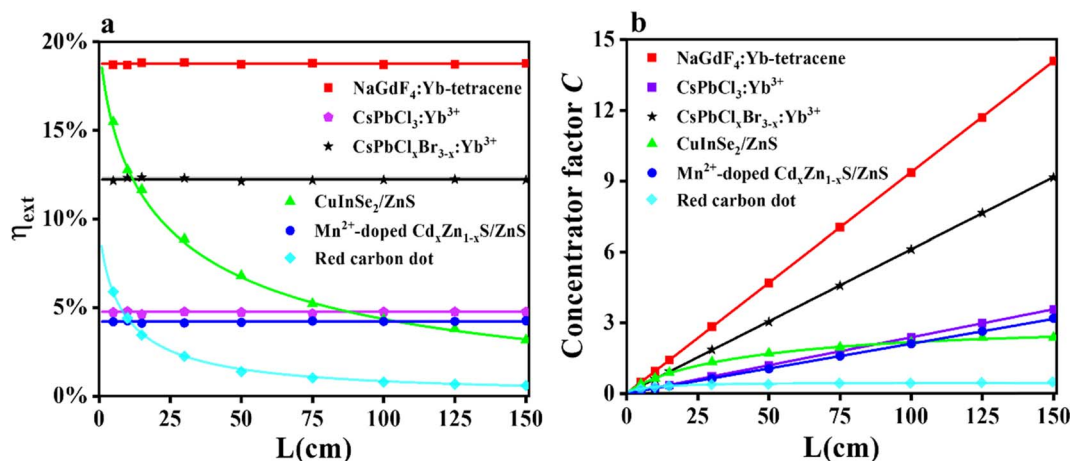

Fig. 4 Monte Carlo ray-tracing simulations of size-dependent η_{ext} under ideal situation (a) and concentration factor C (b) for NaGdF$_4$:Yb–tetracene NCs (red curve and dots), CsPbCl$_3$:Yb^{3+} NCs (purple curve and dots), CsPbCl$_x$Br$_{3-x}$:Yb^{3+} NCs (black curve and dots), CuInSe$_2$/ZnS QDs (green curve and dots), Mn^{2+}-doped Cd$_x$Zn$_{1-x}$S/ZnS QDs (blue curve and dots) and red CDs (cyan curve and dots).

$$C \equiv \frac{B_2}{B_1} \le \frac{v_2^2}{v_1^2} \exp\left(\frac{h(v_1 - v_2)}{KT}\right), \tag{4}$$

where K is the Boltzmann constant, T is the temperature of the medium, B_1 is the input beam's brightness and B_2 is the output beam's brightness. Very recently, Baikie et al. derived the thermodynamic limits of photon-multiplier LSCs[39] as follows:

$$C \equiv \frac{B_2}{B_1} \le \sqrt{\frac{8n^2\pi v_2^4}{B_1 c^2 v_1^2} \exp\left(\frac{h(v_1 - 2v_2)}{KT}\right)}. \tag{5}$$

It is very exciting to find that the concentration factor is closely related to the intensity of the incident light. Subsequently, we bring our simulation objects, NaGdF$_4$:Yb–tetracene-based LSCs and CuInSe$_2$/ZnS-based LSCs, into eqn (4) and (5), respectively. If the emission of these luminophores is narrow enough, the NaGdF$_4$:Yb–tetracene NCs have an emission at hv_2 = 1.253 eV and CuInSe$_2$/ZnS QDs have an emission at hv_2 = 1.459 eV. For NaGdF$_4$:Yb–tetracene-based LSCs, $hv_1 = 2 \times 1.253$ + 0.24 = 2.746 eV, where the value of 0.24 is the thermal loss. For CuInSe$_2$/ZnS-based LSCs, $hv_1 = 1.459 + 0.16 = 1.619$ eV, where the value of 0.16 eV represents the Stokes shift.

The results (Fig. 5) show a significant difference against our real simulations because the thermodynamic concentration limit can reach 10^3 to 10^5 for NaGdF$_4$:Yb–tetracene-based LSCs and 353.5 for CuInSe$_2$/ZnS-based LSCs. Achieving the thermodynamic concentration limit requires an ideal PLQY and an ideal LSC cavity. Moreover, this limiting value is derived under the ideal conditions of single-wavelength light incidence, and emission at the center wavelength, so its value is much larger than our simulation results. The three-dimensional coordinate plot in Fig. 5b further demonstrates the close correlation between the concentrating factor limit of NaGdF$_4$:Yb–tetracene-based LSCs and the PLQY of the luminophores. Therefore, optimizing the efficiency of these luminophores is of paramount importance. Notably, PM-LSCs have a high light-concentration factor in low-brightness environments, whereas QD-based LSCs are not influenced. This remains an important reference for our study although it has not been experimentally confirmed.

(IV) Tandem LSCs

For single-layer LSCs, their efficiency is limited because luminophores with wide bandgaps face the limitation of the absorption efficiency of sunlight while those with narrow bandgaps face the unavoidable thermalization losses caused by the relaxation of high-energy photons to band-edge luminescence. Therefore, tandem LSCs are considered an effective solution for breaking through the efficiency limit. In this work, we choose the NaGdF$_4$:Yb–tetracene-based LSCs as the top layer and CuInSe$_2$/ZnS-based LSCs as the bottom layer (as shown in Fig. 6a). We emphasize that in practical applications, it is the entire system where LSCs are coupled to PVs that need to be investigated rather than just considering the performance of LSCs alone. Thus, EQE$_{LSC-PV}$ and PCE should be studied, and they are strictly required to quantify all PV devices.[40] If a high-performance LSC device is obtained, the alignment between the EQE curve of the PV cell and the PL emission spectrum of the LSC's luminophores significantly impacts the overall energy conversion efficiency. The EQE$_{LSC-PV}$ can be written as follows:

$$EQE_{LSC-PV}(\lambda) = \eta_{ext}(\lambda) \times \frac{\int EQE_{PV}(\lambda') \times \Phi_{PL}(\lambda')d\lambda'}{\int \Phi_{PL}(\lambda')d\lambda'}, \tag{6}$$

$$\eta_{ext} = \frac{\int S_{in}(\lambda) \times \eta_{ext}(\lambda)d\lambda}{\int S_{in}(\lambda)d\lambda}, \tag{7}$$

where $\eta_{ext}(\lambda)$ is the external quantum efficiency under different λ excitations and EQE$_{PV}(\lambda)$ is the external quantum efficiency of PV cells.

For the PCE of the LSC-PV system, due to the inconsistency of the spectrum emitted from the LSC edge with the solar
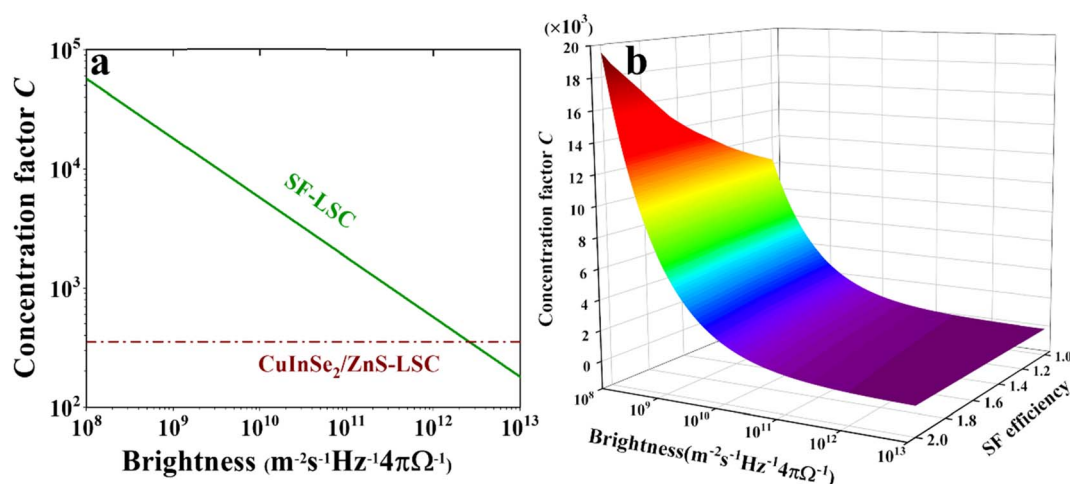

Fig. 5 (a) Thermodynamic limits of concentration factor C for NaGdF$_4$:Yb–tetracene NC-based LSCs (green line) and CuInSe$_2$/ZnS QD-based LSCs (red dash line) at room temperature. (b) Thermodynamic limits of concentration factor C as a function of SF efficiency and input brightness for NaGdF$_4$:Yb–tetracene NC-based LSCs.
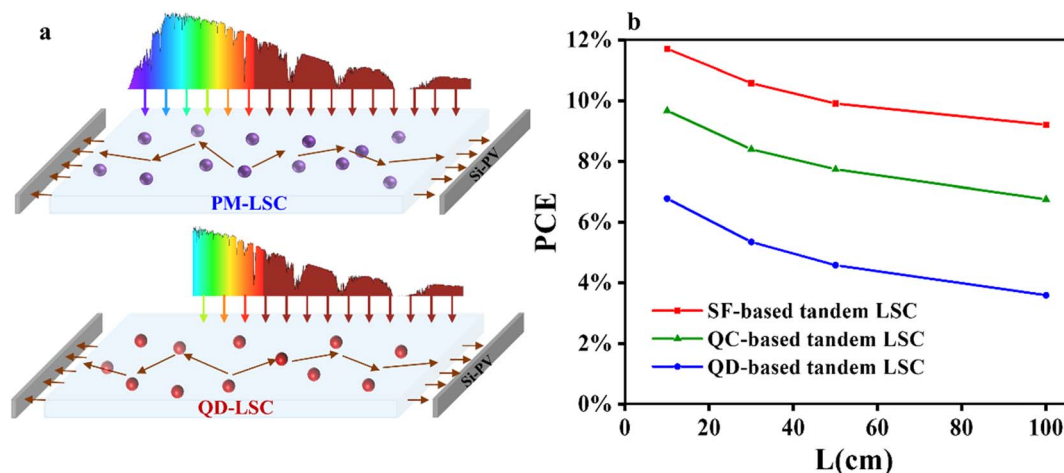
Fig. 6 (a) Schematic representation of tandem LSC-PV systems. (b) Monte Carlo ray-tracing simulations of PCE of tandem LSC-PV systems for different top layer luminophores under ideal situations (red curves represent the NaGdF$_4$:Yb–tetracene NCs, green curves represent the CsPbCl$_x$Br$_{3-x}$:Yb^{3+} NCs, and blue curves represent the Mn^{2+}-doped Cd$_x$Zn$_{1-x}$S/ZnS QDs) while using the CuInSe$_2$/ZnS QDs as bottom layer luminophores.

spectrum, we introduce a spectral shaping factor, q_{LSC}, which is defined as

$$q_{LSC} = \frac{\int EQE_{PV}(\lambda) \times \Phi_{PL}(\lambda)d\lambda / \int \Phi_{PL}(\lambda)d\lambda}{\int EQE_{PV}(\lambda) \times S_{in}(\lambda)d\lambda / \int S_{in}(\lambda)d\lambda}. \quad (8)$$

According to eqn (8), we can estimate the PCE of the system based on the following formula:

$$PCE = q_{LSC}\eta_{ext}\eta_{PV}, \quad (9)$$

where η_{PV} is the PCE of the PV cell. In this work, we use 26.7% of the PCE reported by Yoshikawa et al.[32]

We conducted MC simulations for different L values (10 cm, 30 cm, 50 cm, and 100 cm) under various conditions with optimal PLQY. The top layer luminophores varied from NaGdF$_4$:Yb–tetracene and CsPbCl$_x$Br$_{3-x}$:Yb^{3+} to Mn^{2+}-doped Cd$_x$Zn$_{1-x}$S/ZnS. Notably, the choice of top layer luminophore significantly influences the optimal η_{abs} of the bottom layer. As the absorption capability of the top layer increases, leading to weaker light reaching the bottom layer, the optimal η_{abs} of the bottom layer decreases. Therefore, we change the η_{abs} of bottom LSCs when using different top layer LSCs according to the results shown in Fig. S16.† The results of PCE are shown in Fig. 6b, while those of η_{ext} and EQE$_{LSC-PV}$ are shown in Fig. S17.† If the top layer is Mn^{2+}-doped Cd$_x$Zn$_{1-x}$S/ZnS-based LSCs, the PCE can reach 6.34% when L equals 10 cm, and it decreases to 3.35% when L equals 100 cm. In contrast, if the top layer is CsPbCl$_x$Br$_{3-x}$:Yb^{3+}-based LSCs, the PCE increases to 9% when L equals 10 cm and decreases to 6.28% when L equals 100 cm. The differences in η_{abs} between the two materials are marginal, and the enhancement in efficiency is attributed to photon multiplication. For NaGdF$_4$:Yb–tetracene-based top-layer LSCs, the PCE of a tandem system can reach up to 10.9%, while the η_{ext} reaches 27.55% for $L = 10$ cm. Even though when L equals 100 cm, the PCE can still reach ~9%. If we can further shorten

the half-height width of the emission spectra of the luminophores, the PCE can reach its limit of 11.7%. The tandem LSCs based on SF luminophore show great promise for commercialization, provided that we achieve the optimal PLQY of the luminophore. Our simulation results establish the efficiency limits of LSCs at this stage. Notably, these simulation data were calculated using the methodology assessed by Yang et al., authoritative experts in the field of LSCs.[40]

Conclusion

Through a combination of MC simulation and computational studies, we showed six promising luminophores of LSCs that are representative of the materials most likely to break through the efficiency limit of LSCs. For luminophores with large Stokes shift but still having reabsorption such as CuInSe$_2$/ZnS QD, the constructed LSCs have competitiveness when the area is small. For luminophores without reabsorption, they are quite suitable for large-area LSCs even when L reaches 1 m. Absorption efficiency plays an important role in affecting the η_{ext} of PM-LSCs. Consequently, NaGdF$_4$:Yb–tetracene-based LSCs can achieve a superior η_{ext} of 18.8%, which is much higher than the efficiency reported thus far. Intriguingly, the thermodynamic concentration limit demonstrates that PM-LSCs are more suitable for working in situations of lower incident light intensity. We emphasize that constructing PM-LSCs is one of the most promising ways to break through the efficiency bottleneck of LSCs due to their negligible reabsorption and their capability to multiply the emitted photons. Subsequently, we use NaGdF$_4$:Yb–tetracene-based LSCs in combination with CuInSe$_2$/ZnSbased LSCs to form the tandem LSCs. The η_{ext} of the tandem system reaches 27.55% for $L = 10$ cm, and the PCE exceeds 11% under an ideal situation. Even when L equals 100 cm, the PCE could remain ~9%. We believe that this tandem LSC system can reach the highest efficiency that can be achieved by LSCs based on existing materials. Consequently, it is crucial to work on

This journal is © The Royal Society of Chemistry 2024

J. Mater. Chem. A, 2024, **12**, 19899–19909 | **19907**

improving the PLQY of these luminophores in future studies. To achieve excellent LSC performance under practical situations, the PLQY of the luminophores should be larger than 80%; meanwhile, the PLQY of PM luminophores should be larger than 160%. More luminophores with large Stokes shift and free absorption should be investigated, and the development of highly efficient, large-area LSCs is urgent.

Data availability

The data are available from the corresponding author on reasonable request.

Author contributions

Qi Nie: conceptualization, data curation, investigation, formal analysis, and writing original draft; Wenqing Li: investigation and data curation; Kuilin Li: formal analysis and validation; Xiao Luo: funding acquisition, supervision, and writing – review & editing.

Conflicts of interest

There are no conflicts to declare.

Acknowledgements

Notes and references

1 J. Clarke and J. Searle, *Nat. Energy*, 2021, **6**, 1087–1089.
2 X. Zhu, M. Du, J. Feng, H. Wang, Z. Xu, L. Wang, S. Zuo, C. Wang, Z. Wang, C. Zhang, X. Ren, S. Priya, D. Yang and S. F. Liu, *Angew Chem. Int. Ed. Engl.*, 2021, **60**, 4238–4244.
3 W. H. Weber and J. Lambe, *Appl. Opt.*, 1976, **15**, 2299–2300.
4 R. Olson, R. F. Loring and M. Fayer, *Appl. Opt.*, 1981, **20**, 2934–2940.
5 K. Barnham, J. L. Marques, J. Hassard and P. O'Brien, *Appl. Phys. Lett.*, 2000, **76**, 1197–1199.
6 F. Mateen, S. Y. Lee and S.-K. Hong, *J. Mater. Chem. A*, 2020, **8**, 3708–3716.
7 J. L. Banal, B. Zhang, D. J. Jones, K. P. Ghiggino and W. W. Wong, *Acc. Chem. Res.*, 2017, **50**, 49–57.
8 X. Li, J. Qi, J. Zhu, Y. Jia, Y. Liu, Y. Li, H. Liu, G. Li and K. Wu, *J. Phys. Chem. Lett.*, 2022, **13**, 9177–9185.
9 C. Tummeltshammer, M. Portnoi, S. A. Mitchell, A.-T. Lee, A. J. Kenyon, A. B. Tabor and I. Papakonstantinou, *Nano Energy*, 2017, **32**, 263–270.
10 B. Zhang, P. Zhao, L. J. Wilson, J. Subbiah, H. Yang, P. Mulvaney, D. J. Jones, K. P. Ghiggino and W. W. H. Wong, *ACS Energy Lett.*, 2019, **4**, 1839–1844.
11 B. Zhang, G. Lyu, E. A. Kelly and R. C. Evans, *Adv. Sci.*, 2022, **9**, e2201160.
12 X. Luo, T. Ding, X. Liu, Y. Liu and K. Wu, *Nano Lett.*, 2019, **19**, 338–341.
13 T. A. Cohen, T. J. Milstein, D. M. Kroupa, J. D. MacKenzie, C. K. Luscombe and D. R. Gamelin, *J. Mater. Chem. A*, 2019, **7**, 9279–9288.
14 F. Meinardi, F. Bruni, C. Castellan, M. Meucci, A. M. Umair, M. La Rosa, J. Catani and S. Brovelli, *Adv. Energy Mater.*, 2024, **14**, 2304006.
15 K. Wu, H. Li and V. I. Klimov, *Nat. Photonics*, 2018, **12**, 105–110.
16 K. Gungor, J. Du and V. I. Klimov, *ACS Energy Lett.*, 2022, **7**, 1741–1749.
17 K. Park, J. Yi, S.-Y. Yoon, S. M. Park, J. Kim, H.-B. Shin, S. Biswas, G. Y. Yoo, S.-H. Moon, J. Kim, M. S. Oh, A. Wedel, S. Jeong, H. Kim, S. J. Oh, H. K. Kang, H. Yang and C. J. Han, *Nat. Photonics*, 2024, **18**, 177–185.
18 S. Li, L. Li, H. Tu, H. Zhang, D. S. Silvester, C. E. Banks, G. Zou, H. Hou and X. Ji, *Mater. Today*, 2021, **51**, 188–207.
19 A. Xu, G. Wang, Y. Li, H. Dong, S. Yang, P. He and G. Ding, *Small*, 2020, **16**, e2004621.
20 Y. Li, P. Miao, W. Zhou, X. Gong and X. Zhao, *J. Mater. Chem. A*, 2017, **5**, 21452–21459.
21 Z. Wang, X. Zhao, Z. Guo, P. Miao and X. Gong, *Org. Electron.*, 2018, **62**, 284–289.
22 X. Gong, W. Ma, Y. Li, L. Zhong, W. Li and X. Zhao, *Org. Electron.*, 2018, **63**, 237–243.
23 H. Y. Huang, M. J. Talite, K. B. Cai, R. J. Soebroto, S. H. Chang, W. R. Liu, W. C. Chou and C. T. Yuan, *Nanoscale*, 2020, **12**, 23537–23545.
24 J. Li, J. Chen, X. Zhao, A. Vomiero and X. Gong, *Nano Energy*, 2023, **115**, 108674.
25 K. B. Cai, H. Y. Huang, M. L. Hsieh, P. W. Chen, S. E. Chiang, S. H. Chang, J. L. Shen, W. R. Liu and C. T. Yuan, *ACS Nano*, 2022, **16**, 3994–4003.
26 J. Li, H. Zhao, X. Zhao and X. Gong, *Adv. Funct. Mater.*, 2024, **34**, 2404473.
27 A. Rao and R. H. Friend, *Nat. Rev. Mater.*, 2017, **2**, 17063.
28 V. Gray, Z. Zhang, S. Dowland, J. R. Allardice, A. M. Alvertis, J. Xiao, N. C. Greenham, J. E. Anthony and A. Rao, *J. Phys. Chem. Lett.*, 2020, **11**, 7239–7244.
29 V. Gray, D. T. W. Toolan, S. Dowland, J. R. Allardice, M. P. Weir, Z. Zhang, J. Xiao, A. Klimash, J. F. Winkel, E. K. Holland, G. M. Fregoso, J. E. Anthony, H. Bronstein, R. Friend, A. J. Ryan, R. A. L. Jones, N. C. Greenham and A. Rao, *J. Am. Chem. Soc.*, 2024, **146**, 7763–7770.
30 T. K. Baikie, B. Daiber, E. Kensington, J. Xiao, N. C. Greenham, B. Ehrler and A. Rao, *Joule*, 2024, **8**, 799–816.
31 S. Han, R. Deng, Q. Gu, L. Ni, U. Huynh, J. Zhang, Z. Yi, B. Zhao, H. Tamura, A. Pershin, H. Xu, Z. Huang, S. Ahmad, M. Abdi-Jalebi, A. Sadhanala, M. L. Tang, A. Bakulin, D. Beljonne, X. Liu and A. Rao, *Nature*, 2020, **587**, 594–599.

32 K. Yoshikawa, H. Kawasaki, W. Yoshida, T. Irie, K. Konishi, K. Nakano, T. Uto, D. Adachi, M. Kanematsu, H. Uzu and K. Yamamoto, *Nat. Energy*, 2017, **2**, 17032.

33 T. J. Milstein, K. T. Kluherz, D. M. Kroupa, C. S. Erickson, J. J. De Yoreo and D. R. Gamelin, *Nano Lett.*, 2019, **19**, 1931–1937.

34 Z. Wang, F. Yuan, X. Li, Y. Li, H. Zhong, L. Fan and S. Yang, *Adv. Mater.*, 2017, **29**, 1702910.

35 H. L. Stern, A. Cheminal, S. R. Yost, K. Broch, S. L. Bayliss, K. Chen, M. Tabachnyk, K. Thorley, N. Greenham, J. M. Hodgkiss, J. Anthony, M. Head-Gordon, A. J. Musser, A. Rao and R. H. Friend, *Nat. Chem.*, 2017, **9**, 1205–1212.

36 V. I. Klimov, T. A. Baker, J. Lim, K. A. Velizhanin and H. McDaniel, *ACS Photonics*, 2016, **3**, 1138–1148.

37 X. Liu, D. Benetti, J. Liu, L. Jin and F. Rosei, *Nano Energy*, 2023, **111**, 108438.

38 E. Yablonovitch, *J. Opt. Soc. Am.*, 1980, **70**, 1362–1363.

39 T. K. Baikie, A. Ashoka, A. Rao and N. C. Greenham, *PRX Energy*, 2022, **1**, 033001.

40 C. Yang, H. A. Atwater, M. A. Baldo, D. Baran, C. J. Barile, M. C. Barr, M. Bates, M. G. Bawendi, M. R. Bergren, B. Borhan, C. J. Brabec, S. Brovelli, V. Bulović, P. Ceroni, M. G. Debije, J.-M. Delgado-Sanchez, W.-J. Dong, P. M. Duxbury, R. C. Evans, S. R. Forrest, D. R. Gamelin, N. C. Giebink, X. Gong, G. Griffini, F. Guo, C. K. Herrera, A. W. Y. Ho-Baillie, R. J. Holmes, S.-K. Hong, T. Kirchartz, B. G. Levine, H. Li, Y. Li, D. Liu, M. A. Loi, C. K. Luscombe, N. S. Makarov, F. Mateen, R. Mazzaro, H. McDaniel, M. D. McGehee, F. Meinardi, A. Menéndez-Velázquez, J. Min, D. B. Mitzi, M. Moemeni, J. H. Moon, A. Nattestad, M. K. Nazeeruddin, A. F. Nogueira, U. W. Paetzold, D. L. Patrick, A. Pucci, B. P. Rand, E. Reichmanis, B. S. Richards, J. Roncali, F. Rosei, T. W. Schmidt, F. So, C.-C. Tu, A. Vahdani, W. G. J. H. M. van Sark, R. Verduzco, A. Vomiero, W. W. H. Wong, K. Wu, H.-L. Yip, X. Zhang, H. Zhao and R. R. Lunt, *Joule*, 2022, **6**, 8–15.

This journal is © The Royal Society of Chemistry 2024

J. Mater. Chem. A, 2024, **12**, 19899–19909 | **19909**